Collective excitations and far-infrared optical absorptions in parallel quantum-well wires

1995 J. Phys.: Condens. Matter 7 3539

(http://iopscience.iop.org/0953-8984/7/18/018)

J. Phys.: Condens. Matter 7 (1995) 3539–3555. Printed in the UK

Collective excitations and far-infrared optical absorptions in parallel quantum-well wires

Hong Sun†‡, Yong Liang Liu§ and Kin Wah Yu¶

† CCAST (World Laboratory), PO Box 8730, Beijing 100080, People's Republic of China
‡ Department of Physics and Institute of Condensed Matter Physics, Shanghai Jiao Tong University, Shanghai 200030, People's Republic of China
§ Department of Physics, Shanghai Jiao Tong University, Shanghai 200030, People's Republic of China
¶ Department of Physics, The Chinese University of Hong Kong, Shatin, New Territories, Hong Kong

Received 3 January 1995, in final form 28 February 1995

Abstract. The intrasubband and intersubband plasmons in the long-wavelength limit are calculated numerically for GaAs/AlAs parallel quantum-well wires (PQWW) produced by the deposition of GaAs and AlAs fractional layers on (001) vicinal GaAs substrates. One intrasubband plasmon mode is found, the energy of which approaches zero as the in-plane wave vector $q \to 0$. The dispersion relations of the intrasubband plasmons are anisotropic with $\hbar\omega_p = [(\alpha^2 q_x^2 + \alpha_0^2 q_y^2)/q]^{1/2}$. The constant α_0 increases monotonically with the electron density n_e of the PQWW, while α increases with n_e when the Fermi energy E_F is in the electron conduction subbands; it decreases with n_e when E_F is in the gaps of the subbands. The intersubband plasmons are found to be multi-branch structured with non-zero energies as $q \to 0$. The calculations show that, for the GaAs/AlAs PQWW we consider where the lateral periods L_x of the PQWW are much less than 200 Å, the far-infrared optical absorptions are dominated by single-electron direct transitions between different electron conduction subbands. For PQWW with L_x larger than 300 Å, the absorptions are due to intersubband plasmon absorptions. Between these two regions, both single-electron direct transitions and intersubband plasmon absorptions can make important contributions to the absorptions, depending on the structures of the PQWW.

1. Introduction

In recent years much attention has been focused on a new kind of low-dimensional electronic system, where 2D electronic gases are further modulated by periodic potentials in lateral directions [1–20]. Though the lateral periodic potentials can be two-dimensional, we restrict our discussions in this paper to one-dimensional lateral periodic potentials. Such structures are referred to as lateral surface superlattices (LSSL) or parallel quantum-well wires (PQWW), depending on whether electrons in the system can tunnel easily in the lateral directions (weak potentials) or are localized in separate channels (strong potentials). PQWW (or LSSL) are primarily fabricated with the following methods: (i) by applying gate voltages to periodically structured electrodes laid lithographically on top of the 2D electronic systems [2, 12], (ii) by directly etching the periodic structures on top of quantum-well structures [14, 17], (iii) by deposition of AlAs and GaAs fractional layers on (001) vicinal surfaces of GaAs substrates [4, 11] and (iv) by direct molecular-beam epitaxy growth of GaAs and AlAs layers on high-index GaAs surfaces [20]. The first two methods usually generate PQWW with lateral periods longer than 1000 Å, while the latter two methods can produce lateral

0953-8984/95/183539+17$19.50

periods down to 100 Å or less. Far-infrared (FIR) absorption experiments provide a simple and direct method of testing the effects of lateral periodic potentials on the electronic structures in PQWW. A considerable number of FIR measurements have been performed on PQWW with long lateral periods [17, 21–25]. It is now believed that the measured FIR resonance energies correspond to the energies of the so-called intersubband plasmon modes in PQWW, which arise from the electron–electron interactions between different electron conduction subbands caused by the lateral periodic potentials [26–31] (hereinafter, by the term 'subband', we mean the electron conduction subband). The intersubband plasmons of PQWW are determined mainly by the Fourier component of the electron–electron interaction

$$V(Q) = (2\pi e^2/\epsilon Q) \int dz\, dz'\, |\varphi(z)|^2 |\varphi(z')|^2 e^{-Q|z-z'|}$$

where $Q = 2\pi/L_x$ is the reciprocal lattice wave vector associated with the period L_x of the lateral potentials, and $|\varphi(z)|^2$ is the electron distribution in the direction perpendicular to the PQWW [29, 31]. $V(Q)$ decreases quickly as L_x decreases. Therefore, for PQWW with short lateral periods, the energies of the intersubband plasmons will be very close to the transition energies of the single electrons between different subbands. It is not clear whether the FIR optical absorptions in PQWW with short lateral periods are determined by the intersubband plasmons or by the single-electron transitions between subbands.

Because of the strong absorption strengths, the optical absorptions due to single-electron transitions between subbands in conventional superlattices have been proposed to design carrier-activated light modulators in the FIR regions [32, 33]. The GaAs/AlAs PQWW produced by the deposition of AlAs and GaAs fractional layers on (001) vicinal surfaces of GaAs substrates (method (iii) mentioned above) should be a better candidate for the carrier-activated light modulator and other optoelectronic device designs, due to its strong optical absorptions and the large electro-absorption effects of the subbands. The subband structures of the PQWW are determined by the periodic lateral potentials, which for PQWW produced with vicinal surfaces arise from the periodically structured interfaces. Electric fields applied normally to the PQWW can shift the electrons towards or away from the structured interfaces and so adjust the strengths of the lateral periodic potentials. The electron transition energies between different subbands are easily controlled by the applied electric fields. For practical optoelectronic applications, it is important to know if the FIR optical absorptions of the PQWW produced with vicinal surfaces are from intersubband plasmons or from single-electron transitions between subbands.

In this paper we present the results of a theoretical investigation on the plasmons in the GaAs/AlAs PQWW produced by the deposition of AlAs and GaAs fractional layers on (001) vicinal surfaces of GaAs substrates in the long-wavelength limit. The FIR optical absorptions of the PQWW are calculated with and without electron–electron interactions to determine the plasmon effects on the FIR absorptions of the PQWW. The complicated boundary conditions of the electron wavefunctions on the periodically structured interfaces of the PQWW are dealt with by introducing a coordinate transformation [34] which transforms the PQWW with periodically structured interfaces to those with planar interfaces plus effective lateral periodic potentials. The paper is organized as follows. The subband structures of the PQWW we considered are calculated in the next section. In section 3 we outline the theories of the plasmons and FIR absorptions of the PQWW. Numerical results and discussions are given in the final section.

2. Subband structures in PQWW

The PQWW structure we considered consists of a GaAs well and AlAs barriers separated

by interfaces at $z = \pm L_z/2 + f_\pm(x)$, where L_z is the average width of the well and $f_\pm(x)$ describe the periodic structures on the interfaces. The periodically structured interfaces are assumed to be one-dimensional in the x direction, which are the structures fabricated at present in the experiments. The Hamiltonian of a single electron in the PQWW is

$$H = -\frac{\hbar^2}{2m_e}\nabla_r^2 + V(\boldsymbol{r}) \tag{1}$$

where $m_e = 0.0665m_0$ is the conduction electron band mass in GaAs and $V(\boldsymbol{r})$ is the electron potential that confines the electron in the well of the PQWW; $V(\boldsymbol{r})$ is given by

$$V(\boldsymbol{r}) = \begin{cases} 0 & -L_z/2 + f_-(x) < z < L_z/2 + f_+(x) \\ \infty & \text{otherwise.} \end{cases} \tag{2}$$

Because of the large conduction band offset between GaAs and AlAs, in equation (2) we have assumed that the potential barriers on the interfaces are infinitely high. The solutions of the eigenenergies and wavefunctions of the single electron are complicated by the boundary conditions that the electron wavefunction must satisfy on the periodically structured interfaces at $z = \pm L_z/2 + f_\pm(x)$. We avoid this difficulty by introducing the following coordinate transformation [34]:

$$\begin{aligned} \tilde{x} &= x \\ \tilde{y} &= y \\ \tilde{z} &= L_z\{z - [f_+(x) + f_-(x)]/2\}/[L_z + f_+(x) - f_-(x)] \end{aligned} \tag{3}$$

which transforms the PQWW in the space $\boldsymbol{r}$ into a quantum well with planar interfaces at $\tilde{z} = \pm L_z/2$ in the space $\tilde{\boldsymbol{r}}$. The boundary conditions of the electron wavefunctions are greatly simplified, while the effective Hamiltonian of a single electron in the transformed space $\tilde{\boldsymbol{r}}$ can be written formally as

$$H_{\text{eff}}(\tilde{\boldsymbol{r}}) = H_0(\tilde{\boldsymbol{r}}) + H_1(\tilde{\boldsymbol{r}}) \tag{4}$$

where H_0 is the Hamiltonian of a GaAs quantum well with planar interfaces and H_1 is a lateral periodic potential due to the periodically structured interfaces. The wavefunction of a single electron is written as the superposition of the eigenwavefunctions of H_0:

$$\psi_{nk}(\tilde{\boldsymbol{r}}) = \sum_{l=0}^{\infty}\sum_{m=-\infty}^{\infty} A_{lm}^{(n)}(\boldsymbol{k})\varphi_l(\tilde{z})e^{i[(k_x - Q_m)\tilde{x} + k_y\tilde{y}]}\Big/\sqrt{S_0} = \sum_{lm} A_{lm}^{(n)}(\boldsymbol{k})\varphi_{lm}(\tilde{\boldsymbol{r}}, \boldsymbol{k}) \tag{5}$$

where S_0 is the area of the PQWW surface, $\boldsymbol{k}$ is the in-plane wave vector of a single electron limited within the first Brillouin zone (FBZ), $Q_m = 2\pi m/L_x$ $(m = 0, \pm 1, \pm 2, \ldots)$ is the reciprocal lattice wave vector associated with the lateral period L_x of the PQWW and $\varphi_l(\tilde{z})$ is the lth eigenwavefunction of H_0 in the z direction. The subband energy, $E_n(\boldsymbol{k})$, of a single electron is determined by the following equation:

$$\det|\langle\varphi_{lm}(\tilde{\boldsymbol{r}}, \boldsymbol{k})|H_{\text{eff}}(\tilde{\boldsymbol{r}}) - E_n(\boldsymbol{k})J(\tilde{\boldsymbol{r}})|\varphi_{l'm'}(\tilde{\boldsymbol{r}}, \boldsymbol{k})\rangle| = 0 \tag{6}$$

where

$$J(\tilde{\boldsymbol{r}}) = J(\tilde{x}) = 1 + [f_+(\tilde{x}) - f_-(\tilde{x})]/L_z$$

is the Jacobian determinant associated with the coordinate transformation (3). Because of the translational symmetry of the PQWW in the y direction, the energy of a single electron can be written as $E_n(k) = E_n(k_x) + \hbar^2 k_y^2/2m_e$. The numerical calculation of (6) is carried out by limiting the infinite summation of $\psi_{nk}(\vec{r})$ in (5) to $l = 1, 2, \cdots, L_0$ and $m = 0, \pm 1, \pm 2, \cdots, \pm M_0$. The interface structures of the PQWW depend sensitively on the conditions under which these PQWW are grown. In most work reported in the literature, one of the interfaces of the PQWW is step-shaped, with a step height equal to 2.83 Å. Because the electrons are distributed mainly in the centre of the well, the effect of these small steps on the electrons can be neglected. As a consequence, one of the interfaces of the PQWW can be assumed to be planar. Under ideal conditions, another interface of the PQWW is square-well shaped. But due to the lateral migration of the Ga and As atoms during the growth process [4], the actual profile of the interface is much flattened. As we do not know at present the exact shape of the interface structure, for a model calculation we assume the following simplest interface structure for the PQWW under consideration:

$$f_+(x) = \delta L_z \sin(2\pi x/L_x) \qquad f_-(x) = 0. \tag{7}$$

In table 1 we give the calculated results of the first five subband energies at $k = 0$ and $k = (Q/2, 0)$ for the GaAs/AlAs PQWW with different L_0 and M_0. The structural parameters of the PQWW are $L_z = 100$ Å, $L_x = 200$ Å, and $\delta L_z = 50$ Å. From table 1 we find that, for the first five subbands, it is sufficient to limit $L_0 = 5$ and $M_0 = 5$. The error caused by this approximation is expected to be less than 0.5%. In figure 1 we give the calculated energies $E_n(k_x)$ as a function of the reduced wave vector k_x/Q ($Q = 2\pi/L_x$) for the GaAs/AlAs PQWW with $L_z = 100$ Å, $L_x = 200$ Å, and (*a*) $\delta L_z = 0$ Å, (*b*) $\delta L_z = 10$ Å, (*c*) $\delta L_z = 30$ Å and (*d*) $\delta L_z = 50$ Å. The subband structure changes greatly as the amplitude of the interface structure changes. In figures 2 and 3, we give the calculated subband width, $W_n = \max\{E_n(k_x)\} - \min\{E_n(k_x)\}$, and the subband gap, $\delta E_n = \min\{E_n(k_x) - E_{n-1}(k_x)\}$, as a function of the reduced amplitude $\delta L_z/L_z$ of the interface structures of the same PQWW as that in figure 1.

Table 1. Numerical results for the conduction subband energy dispersions $E_n(k_x)$ of single electrons in the GaAs/AsAl PQWW with $L_z = 100$ Å, $L_x = 200$ Å and $\delta L_z = 50$ Å. The calculations were carried out at the centre ($k_x/Q = 0$) and edge ($k_x/Q = 0.5$) of the first Brillouin zone, with $Q = 2\pi/L_x$ the reciprocal lattice wave vector associated with the lateral period L_x of the PQWW; $L_0 \times (2M_0 + 1)$ expansion wavefunctions (see the text) were used in the calculations. Energy is measured in meV.

		$E_0(k_x)$	$E_1(k_x)$	$E_2(k_x)$	$E_3(k_x)$	$E_4(k_x)$
$k_x/Q = 0$	$L_0 = 1, M_0 = 5$	67.38	154.8	211.9	350.1	352.0
	$L_0 = 2, M_0 = 2$	63.82	140.7	159.1	211.5	296.1
	$L_0 = 3, M_0 = 3$	63.63	139.9	153.8	207.9	272.2
	$L_0 = 4, M_0 = 4$	63.58	139.8	153.3	207.4	270.3
	$L_0 = 5, M_0 = 5$	63.56	139.8	153.1	207.3	269.9
$k_x/Q = 0.5$	$L_0 = 1, M_0 = 5$	67.84	148.1	246.3	268.1	474.9
	$L_0 = 2, M_0 = 2$	64.31	134.4	165.2	243.1	255.5
	$L_0 = 3, M_0 = 3$	64.07	133.5	157.9	235.8	239.4
	$L_0 = 4, M_0 = 4$	64.02	133.4	157.2	234.7	238.0
	$L_0 = 5, M_0 = 5$	64.00	133.4	157.0	234.5	237.8

The following two points are noteworthy from these numerical results. First, the bandwidths of the subbands, particularly for the first three subbands, reduce quickly as the

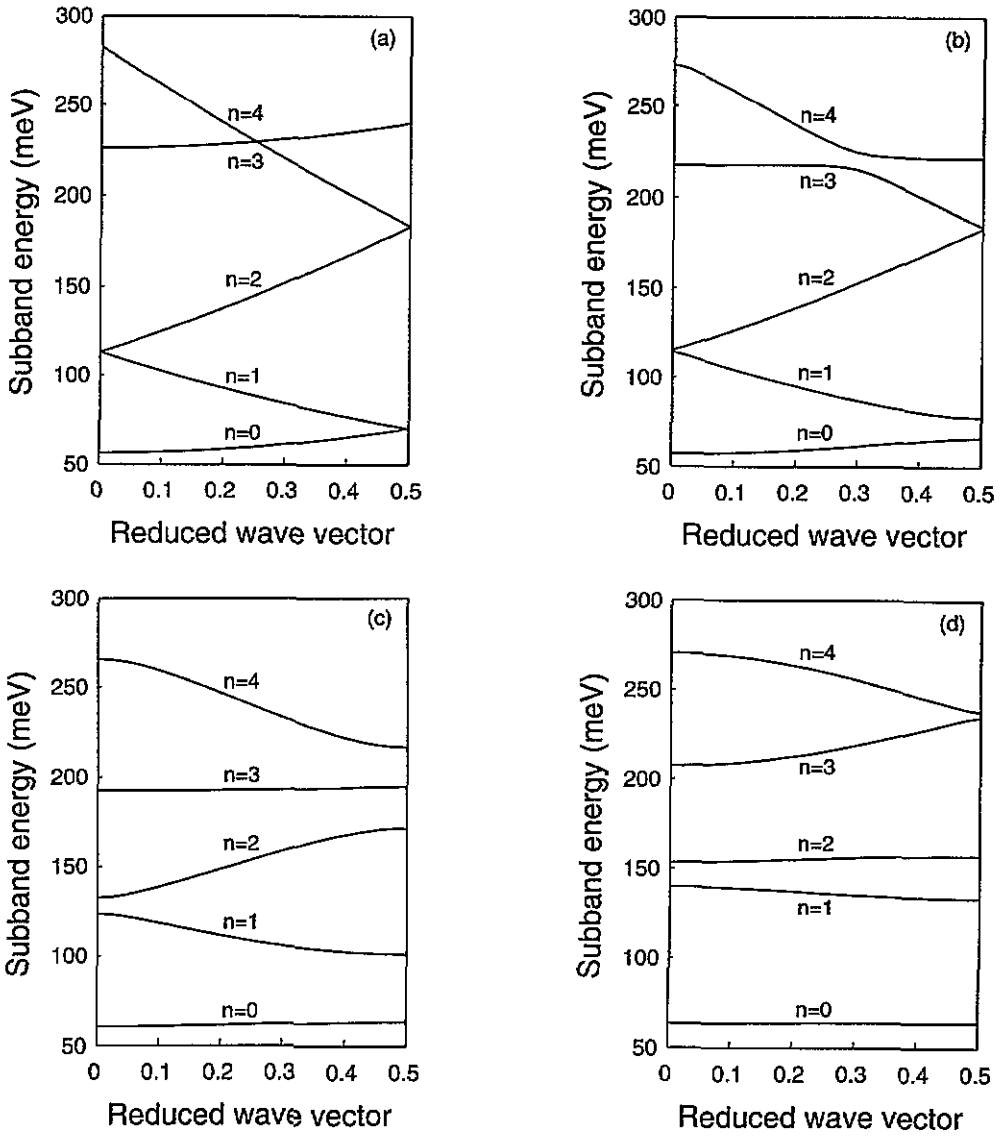

Figure 1. The energies $E_n(k_x)$ of the electron conduction subbands as a function of the reduced wave vector k_x/Q ($Q = 2\pi/L_x$) for GaAs/AlAs PQWW with structural parameters $L_z = 100$ Å, $L_x = 200$ Å, and (*a*) $\delta L_z = 0$ Å, (*b*) $\delta L_z = 10$ Å, (*c*) $\delta L_z = 30$ Å and (*d*) $\delta L_z = 50$ Å.

amplitudes δL_z of the interface structures increase, which indicates a reduced overlapping of the electron wavefunctions between the different quantum-well wires. The electrons are localized in the separate channels for those PQWW with large interface structures. Second, the energy gaps of the subbands increase quickly as δL_z increases. Our calculation will show later that a strong peak appears in the FIR optical absorption spectra of the single electrons associated with the electron transitions across the first subband gap δE_1 at the edge of the FBZ. By changing the structural parameters (δL_z, L_z and L_x) of the PQWW, we can shift this absorption peak from 100 μm to 10 μm in the FIR region.

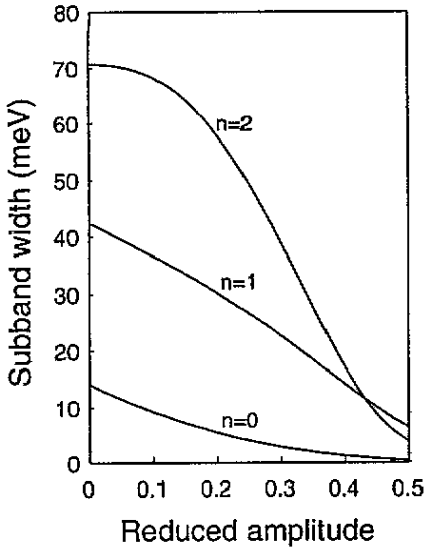

Figure 2. The band widths, $W_n = \max\{E_n(k_x)\} - \min\{E_n(k_x)\}$, of the electron conduction subbands as a function of the reduced amplitude $\delta L_z/L_z$ of the periodically structured interfaces of the same PQWW as that in figure 1.

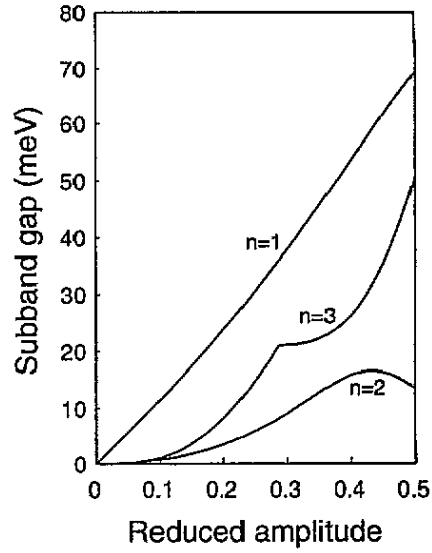

Figure 3. The band gaps, $\delta E_n = \min\{E_n(k_x) - E_{n-1}(k_x)\}$, of the electron conduction subbands as a function of the reduced amplitude $\delta L_z/L_z$ of the periodically structured interfaces of the same PQWW as that in figure 1.

3. Plasmons and FIR absorptions in PQWW

We obtain the plasmons in the PQWW by calculating the electric conductivity of the system. The electric current density $\boldsymbol{j}(\boldsymbol{r},t) = \int \mathrm{d}\omega \boldsymbol{j}(\boldsymbol{r},\omega)\mathrm{e}^{-\mathrm{i}\omega t}$ induced by the electric field $\boldsymbol{E}(\boldsymbol{r},t) = \int \mathrm{d}\omega \boldsymbol{E}(\boldsymbol{r},\omega)\mathrm{e}^{-\mathrm{i}\omega t}$ acting upon the PQWW is given by

$$j_\alpha(\boldsymbol{r},\omega) = \mathrm{i}\frac{N_e e^2}{m_e \omega} E_\alpha(\boldsymbol{r},\omega) + \frac{1}{\omega}\sum_\beta \int \mathrm{d}\boldsymbol{r}'\mathrm{d}(t-t')\frac{\theta(t-t')}{\hbar}\mathrm{e}^{\mathrm{i}\omega(t-t')}\langle[\hat{j}_{H\alpha}(\boldsymbol{r},t)\,,\,\hat{j}_{H\beta}(\boldsymbol{r}',t')]\rangle E_\beta(\boldsymbol{r}',\omega) \tag{8}$$

where N_e is the average electron density per volume of the PQWW and $\hat{j}_H(\boldsymbol{r},t)$ is the electric current density operator. The first term on the right-hand side of (8) represents an imaginary conductivity that contains no information on the plasmons and does not contribute to the FIR absorptions of the PQWW. Strictly speaking, the imaginary part of the conductivity will affect the FIR absorptions by changing the refractive index of the system. But this effect can be included by considering the Kramers–Kronig relations between the real and imaginary parts of the dielectric constant. In what follows, therefore, we neglect this term in (8). It is convenient to work in the transformed space $\tilde{\boldsymbol{r}}$, where the interfaces of the PQWW are planes and the wavefunctions of the single electrons are given by (5). We have

$$j_\alpha^{\mathrm{eff}}(\tilde{\boldsymbol{r}},\omega) = \sum_\beta \int \mathrm{d}\tilde{\boldsymbol{r}}'\sigma_{\alpha\beta}^{\mathrm{eff}}(\tilde{\boldsymbol{r}},\tilde{\boldsymbol{r}}',\omega)\tilde{E}_\beta(\tilde{\boldsymbol{r}}',\omega) \tag{9}$$

and

$$\sigma_{\alpha\beta}^{\mathrm{eff}}(\tilde{r},\tilde{r}',\omega)=\int \mathrm{d}(t-t')\frac{\theta(t-t')}{\hbar}\mathrm{e}^{\mathrm{i}\omega(t-t')}\left\langle\left[\hat{j}_{H\alpha}^{\mathrm{eff}}(\tilde{r},t)\,,\ \hat{j}_{H\beta}^{\mathrm{eff}}(\tilde{r}',t')\right]\right\rangle \tag{10}$$

where we define

$$j_{\alpha}^{\mathrm{eff}}(\tilde{r},\omega)=J(\tilde{r})\tilde{j}_{\alpha}(\tilde{r},\omega)\qquad \hat{j}_{H\alpha}^{\mathrm{eff}}(\tilde{r},t)=J(\tilde{r})\hat{\tilde{j}}_{H\alpha}(\tilde{r},t). \tag{11}$$

In the above expressions $\tilde{j}_{\alpha}(\tilde{r},\omega)$ is the α ($\alpha=x,y,z$) component of the transformed electric current density, etc. For FIR optical absorptions, the wave vector of the electric fields can be neglected in the long-wavelength limit ($q\to 0$). We take $\boldsymbol{E}(\boldsymbol{r},t)=\boldsymbol{e}E_0(\omega)\mathrm{e}^{-\mathrm{i}\omega t}+\boldsymbol{e}E_0^*(\omega)\mathrm{e}^{\mathrm{i}\omega t}$, where the spatial modulation of the electric field is also neglected. The FIR optical absorption coefficient is defined by the average energy absorbed by the PQWW per unit time and volume divided by the average energy incident on the PQWW per unit time and area [35], which is given by

$$\alpha(\omega)=\frac{4\pi}{n(\omega)cV_0}\sum_{\alpha\beta}e_{\alpha}e_{\beta}\mathrm{Re}\left(\sigma_{\alpha\beta}^{\mathrm{eff}}(\omega)\right) \tag{12}$$

where $n(\omega)$ is the refractive index of the PQWW. In the random-phase approximation, the electric conductivity of the PQWW is given by

$$\sigma_{\alpha\beta}^{\mathrm{eff}}(q,\omega)=\sigma_{\alpha\beta}^{(0)}(q,\omega)+\frac{\mathrm{i}}{\omega}T_{\alpha}(q,\omega+\mathrm{i}0^+)[1-V(q)\chi^{(0)}(q,\omega)]^{-1}V(q)[T_{\beta}^*(q,\omega-\mathrm{i}0^+)]^{\mathrm{t}} \tag{13}$$

where

$$\sigma_{\alpha\beta}^{(0)}(q,\omega)=\frac{\mathrm{i}}{\omega}\sum_{nn'k}j_{nk,n'k+q}^{\alpha}(q)j_{nk,n'k+q}^{\beta *}(q)\frac{N_{nk}-N_{n'k+q}}{E_n(k)-E_{n'}(k+q)+\hbar\omega+\mathrm{i}0^+}. \tag{14}$$

The column vector $T_{\alpha}(q,\omega+\mathrm{i}0^+)=\left\{T_{\alpha}^{(l_1l_2)}(q+Q_m,\omega+\mathrm{i}0^+)\right\}$ with

$$T_{\alpha}^{(l_1l_2)}(q+Q_m,\omega+\mathrm{i}0^+)=\sum_{nn'k}j_{nk,n'k+q}^{\alpha}(q)A_{nk,n'k+q}^{(l_1l_2)\,*}(q+Q_m)\times\frac{N_{nk}-N_{n'k+q}}{E_n(k)-E_{n'}(k+q)+\hbar\omega+\mathrm{i}0^+}. \tag{15}$$

The matrix $V(q)=\left\{V_{l_1l_2,l_1'l_2'}(q+Q_m,q+Q_m')\right\}$ with

$$V_{l_1l_2,l_1'l_2'}(q+Q_m,q+Q_m')=\sum_{Q_n}\frac{2\pi e^2}{\epsilon S_0}\int \mathrm{d}\tilde{z}\mathrm{d}\tilde{z}'\varphi_{l_1}(\tilde{z})\varphi_{l_2}^*(\tilde{z})\varphi_{l_1'}^*(\tilde{z}')\varphi_{l_2'}(\tilde{z}')\times\int_0^{L_x}\frac{\mathrm{d}\tilde{x}}{L_x}\frac{\mathrm{d}\tilde{x}'}{L_x}\mathrm{e}^{\mathrm{i}Q_n(\tilde{x}-\tilde{x}')}\mathrm{e}^{-\mathrm{i}(Q_m-Q_m')\tilde{x}'}\frac{\mathrm{e}^{-|q+Q_m+Q_n||\tilde{z}+\delta(\tilde{x},\tilde{z})-\tilde{z}'-\delta(\tilde{x}',\tilde{z}')|}}{|q+Q_m+Q_n|} \tag{16}$$

and the matrix $\chi^{(0)}(q,\omega)=\left\{\chi_{l_1l_2,l_1'l_2'}^{(0)}(q+Q_m,q+Q_m',\omega)\right\}$ with

$$\chi_{l_1l_2,l_1'l_2'}^{(0)}(q+Q_m,q+Q_m',\omega)=\sum_{nn'k}A_{nk,n'k+q}^{(l_1l_2)}(q+Q_m)A_{nk,n'k+q}^{(l_1'l_2')\,*}(q+Q_m')\times\frac{N_{nk}-N_{n'k+q}}{E_n(k)-E_{n'}(k+q)+\hbar\omega+\mathrm{i}0^+} \tag{17}$$

with $N_{nk} = 2/\{\exp[\beta(E_n(k) - \mu)] + 1\}$ the electron Fermi distribution function for the electron in the subband $E_n(k)$, ϵ the static dielectric constant of the PQWW, $\delta(\tilde{x}, \tilde{z}) = (\tilde{z}/L_z)[f_+(\tilde{x}) - f_-(\tilde{x})] + [f_+(\tilde{x}) + f_-(\tilde{x})]/2$, $Q_m = (Q_m, 0, 0)$

$$A^{(l_1 l_2)}_{nk,n'k+q}(q + Q_m) = \int d\tilde{\rho} e^{-i(q+Q_m)\cdot\tilde{\rho}} J(\tilde{x}) \psi^{(l_1)*}_{nk}(\tilde{\rho}) \psi^{(l_2)}_{n'k+q}(\tilde{\rho}) \tag{18}$$

and

$$j^{\alpha}_{nk,n'k+q}(q) = -\frac{e}{2m_e} \int d\tilde{r} e^{-iq\cdot\tilde{\rho}} J(\tilde{x}) \left[\psi^{*}_{nk}(\tilde{r}) P_\alpha(\tilde{r}) \psi_{n'k+q}(\tilde{r}) - \psi_{n'k+q}(\tilde{r}) P_\alpha(\tilde{r}) \psi^{*}_{nk}(\tilde{r})\right] \tag{19}$$

where $P(\tilde{r})$ is the electron momentum operator in the transformed space $\tilde{r}$ and $\psi^{(l)}_{nk}(\tilde{\rho})$ is defined from (5) by

$$\psi^{(l)}_{nk}(\tilde{\rho}) = \sum_{m=-\infty}^{\infty} A^{(n)}_{lm}(k) e^{i[(k_x - Q_m)\tilde{x} + k_y \tilde{y}]} \Big/ \sqrt{S_0}. \tag{20}$$

In (13), $\sigma^{(0)}_{\alpha\beta}(q, \omega)$ represents the contribution to the electric conductivity of the single-electron transitions, while the second term on the right-hand side of (13) is the effect from the plasmons of the PQWW. The energies of the plasmons in the PQWW are determined by the poles of the matrix $[1 - V(q)\chi^{(0)}(q, \omega)]^{-1}$, i.e. by the solutions of the following equation:

$$\det\left|1 - V(q)\,\chi^{(0)}(q, \omega)\right| = 0. \tag{21}$$

In the long-wavelength limit ($q \to 0$), we can divide the matrix $V(q)$ into

$$V_{l_1 l_2, l_1' l_2'}(q + Q_m, q + Q'_m) = \frac{2\pi e^2}{\epsilon S_0 q} \delta_{l_1, l_2} \delta_{l_1', l_2'} \delta_{m,0} \delta_{m',0} + \tilde{V}_{l_1 l_2, l_1' l_2'}(q + Q_m, q + Q'_m) \tag{22}$$

where $\tilde{V}_{l_1 l_2, l_1' l_2'}(q + Q_m, q + Q'_m)$ is finite as $q \to 0$. Neglecting contributions to the plasmon energies from terms with orders of magnitudes higher than $\sqrt{q}$ in the long-wavelength limit ($q \to 0$), we obtain from (21) two sets of plasmon modes, which are determined by the following equation (see the appendix):

$$\left(1 - \frac{2\pi e^2}{\epsilon S_0 q} \sum_{ll'} \chi^{(0)}_{ll,l'l'}(q, q, \omega)\right) \det\left|1 - \tilde{V}(q)\,\chi^{(0)}(q, \omega)\right| = 0. \tag{23}$$

The solutions of the first factor in (23) determine the energies of the so-called intrasubband plasmons, while those of the second factor, which is obtained from (21) by replacing $V(q) = \{V_{l_1 l_2, l_1' l_2'}(q + Q_m, q + Q'_m)\}$ with $\tilde{V}(q) = \{\tilde{V}_{l_1 l_2, l_1' l_2'}(q + Q_m, q + Q'_m)\}$, determine the energies of the intersubband plasmons of the PQWW. The numerical results are given in the next section.

4. Results and discussions

4.1. Intrasubband plasmons

In the long-wavelength limit ($q \to 0$), the energies of the intrasubband plasmons are determined by the solutions of the following equation:

$$\left(1 - \frac{2\pi e^2}{\epsilon S_0 q} \sum_{ll'} \chi^{(0)}_{ll',l'l'}(q, q, \omega)\right) = 0. \tag{24}$$

The intrasubband plasmons arise from the electron interactions within the same subbands of the PQWW. From the definition of $A^{ll}_{nk,n'k+q}(q)$, equation (18), we have

$$\begin{aligned}\sum_{l=0}^{\infty} A^{ll}_{nk,n'k+q}(q) &= \sum_{l=0}^{\infty} \int \mathrm{d}\tilde{\rho} J(\tilde{x}) \psi^{(l)}_{nk}(\tilde{\rho}) \mathrm{e}^{-\mathrm{i}q\cdot\tilde{\rho}} \psi^{(l)}_{n'k+q}(\tilde{\rho}) \\ &= \sum_{l=0}^{\infty} \int \mathrm{d}\tilde{\rho} J(\tilde{x}) \psi^{(l)}_{nk}(\tilde{\rho}) \psi^{(l)}_{n'k}(\tilde{\rho}) + \mathrm{O}(q) = \delta_{n,n'} + \mathrm{O}(q). \end{aligned} \tag{25}$$

The second equality in (25) is obtained by expanding $\mathrm{e}^{-\mathrm{i}q\cdot\tilde{\rho}} \psi^{(l)}_{n'k+q}(\tilde{\rho})$ as a function of q, and the last equality is obtained from the orthonormalization relation of the single-electron wavefunction:

$$\begin{aligned}\int \mathrm{d}r \psi^*_{nk}(r) \psi_{n'k'}(r) &= \int \mathrm{d}\tilde{r} J(\tilde{r}) \psi^*_{nk}(\tilde{r}) \psi_{n'k'}(\tilde{r}) \\ &= \sum_{l=0}^{\infty} \int \mathrm{d}\tilde{\rho} J(\tilde{x}) \psi^{(l)}_{nk}(\tilde{\rho}) \psi^{(l)}_{n'k'}(\tilde{\rho}) = \delta_{n,n'} \delta_{k,k'}. \end{aligned} \tag{26}$$

With (25) it is easy to show, from (17), (18) and (24), that the contributions to the energies of the intrasubband plasmons from the electron interactions between different subbands are at least proportional to q. Neglecting electron interactions between different subbands we obtain only one intrasubband plasmon mode, with its energy given by

$$\hbar\omega_{\mathrm{p}} = \left[(\alpha^2 q_x^2 + \alpha_0^2 q_y^2)/q\right]^{1/2}$$

with $q = \sqrt{q_x^2 + q_y^2}$ and

$$\alpha_0^2 = \frac{4\pi e^2}{\epsilon} \sqrt{2\frac{\hbar^2}{m_{\mathrm{e}}}} \sum_n \int_0^{k_{\mathrm{F}}^{(n)}} \frac{\mathrm{d}k_x}{\pi^2} \sqrt{E_{\mathrm{F}} - E_n(k_x)} = \frac{2\pi e^2 n_{\mathrm{e}} \hbar^2}{\epsilon m_{\mathrm{e}}} \tag{27}$$

$$\alpha^2 = \frac{4\pi e^2}{\epsilon} \sqrt{2\frac{m_{\mathrm{e}}}{\hbar^2}} \sum_n \int_0^{k_{\mathrm{F}}^{(n)}} \frac{\mathrm{d}k_x}{\pi^2} \sqrt{E_{\mathrm{F}} - E_n(k_x)} \frac{\mathrm{d}^2 E_n(k_x)}{\mathrm{d}k_x^2}. \tag{28}$$

The summation is over all the occupied subbands, n_{e} is the electron density per area of the PQWW and the wave vector $k_{\mathrm{F}}^{(n)}$ is determined by

$$\begin{aligned} &k_{\mathrm{F}}^{(n)} = 0 \qquad E_{\mathrm{F}} < \min\{E_n(k_x)\} \\ &E_{\mathrm{F}} = E_n(k_{\mathrm{F}}^{(n)}) \qquad \min\{E_n(k_x)\} < E_{\mathrm{F}} < \max\{E_n(k_x)\} \\ &k_{\mathrm{F}}^{(n)} = \pi/Lx \qquad \max\{E_n(k_x)\} < E_{\mathrm{F}}. \end{aligned} \tag{29}$$

Because the constant α depends on the second derivative of $E_n(k_x)$, it results in a sensitive dependence of α on the dispersion relation of $E_n(k_x)$ and thus on the interface structures of the PQWW. If the interfaces are planes $[f_\pm(x) = 0]$, we have $d^2E_n(k_x)/dk_x^2 = \hbar^2/m_e$ and $\alpha \to \alpha_0$. Equation (27) gives the dispersion relation of the intrasubband plasmons in conventional quantum wells. If the amplitudes of the interface structures of the PQWW are large, $E_n(k_x)$ is almost constant (see figure 1) and $\alpha \to 0$. Equation (27) gives a strong anisotropic dispersion relation of the intrasubband plasmons. In figure 4, the anisotropic parameter $\gamma = \alpha/\alpha_0$ is calculated as a function of the reduced amplitude $\delta L_z/L_z$ for the GaAs/AlAs PQWW with the interface structures given by (7) and the structural parameters $L_z = 100\,\text{Å}$ and $L_x = 200\,\text{Å}$. The electron densities in figure 4 are $n_1 = 1 \times 10^{11}\,\text{cm}^{-2}$, $n_2 = 2 \times 10^{11}\,\text{cm}^{-2}$ and $n_3 = 3 \times 10^{11}\,\text{cm}^{-2}$. In figure 5, γ is given as a function of the electron density n_e for the same PQWW as that in figure 4, with (i) $\delta L_z = 10\,\text{Å}$, (ii) $\delta L_z = 30\,\text{Å}$ and (iii) $\delta L_z = 50\,\text{Å}$.

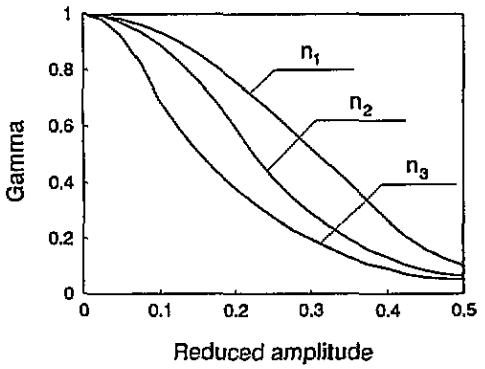

Figure 4. The anisotropic parameter $\gamma = \alpha/\alpha_0$ of the intrasubband plasmons (defined in the text) is given as a function of the reduced amplitude $\delta L_z/L_z$ of the periodically structured interfaces of the GaAs/AlAs PQWW with the structural parameters $L_z = 100\,\text{Å}$ and $L_x = 200\,\text{Å}$. The electron densities are $n_1 = 1 \times 10^{11}\,\text{cm}^{-2}$, $n_2 = 2 \times 10^{11}\,\text{cm}^{-2}$ and $n_3 = 3 \times 10^{11}\,\text{cm}^{-2}$.

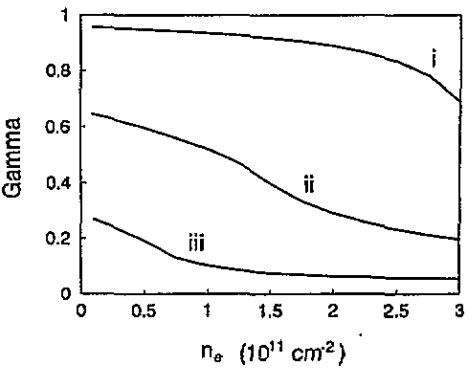

Figure 5. The anisotropic parameter $\gamma = \alpha/\alpha_0$ of the intrasubband plasmons is given as a function of the electron density n_e for the same PQWW as that in figure 4 with (i) $\delta L_z = 10\,\text{Å}$, (ii) $\delta L_z = 30\,\text{Å}$ and (iii) $\delta L_z = 50\,\text{Å}$.

If we set $q_y = 0$ in (27), the energy of the intrasubband plasmon is $\hbar\omega_p = \alpha\sqrt{|q_x|}$. In figure 6 we give the calculated constant $\alpha/\alpha_0^{(0)}$ as a function of the electron density n_e for the PQWW with $L_z = 100\,\text{Å}$, $L_x = 200\,\text{Å}$ and $\delta L_z = 30\,\text{Å}$. Also given in figure 6 is the calculated constant $\alpha_0/\alpha_0^{(0)}$, where α_0 (equation (28)) equals the intrasubband plasmon constant in a quantum well with planar interfaces and a width equal to L_z; $\alpha_0^{(0)}$ is obtained from α_0 with the electron density fixed at $n_e = 1 \times 10^{11}\,\text{cm}^{-2}$. The first broken line on the low-energy side in figure 6 indicates the electron density at which the lowest subband is just filled up with the electrons, or with $E_F = \max\{E_0(k_x)\}$, and the second broken line in figure 6 gives the electron density at which the electrons begin to fill the second subband, or with $E_F = \min\{E_1(k_x)\}$. It is interesting to note from figures 4–6 that γ decreases monotonically as n_e increases, while α increases with n_e when the Fermi level E_F lies within the subbands, and it decreases with n_e when E_F is shifted into the gaps of the subbands. This oscillatory behaviour of the intrasubband plasmon frequencies as a function of E_F, or equivalently n_e, has been predicted before for quantum-dot array systems [36].

The results in figure 6 also show that, for the same electron density n_e and wave vector q, the energy of the intrasubband plasmon in the PQWW is less than that in the quantum well with planar interfaces and a width equal to the average width of the PQWW. The intrasubband plasmons do not affect the FIR optical absorptions since their energies approach zero as $q \to 0$. Other optical techniques, such as Raman scattering, are needed to detect the intrasubband plasmons in the PQWW.

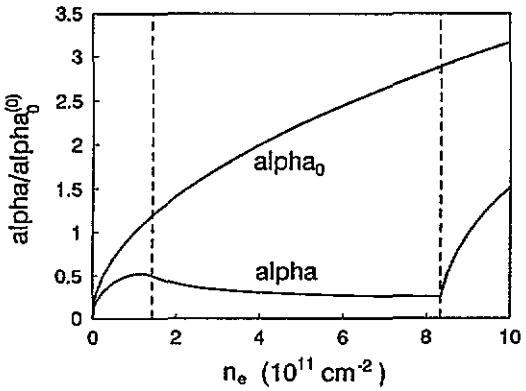

Figure 6. The intrasubband plasmon constants α and α_0 defined in the text are given as a function of the electron density n_e for the GaAs/AlAs PQWW with structural parameters $L_z = 100$ Å, $L_x = 200$ Å and $\delta L_z = 30$ Å. The results are divided by $\alpha_0^{(0)}$, which is obtained from α_0 with the electron density fixed at $n_e = 1 \times 10^{11}$ cm^{-2}. The first broken line on the low-energy side indicates the electron density at which the lowest electron conduction subband is just filled up with the electrons, or with $E_F = \max\{E_0(k_x)\}$, and the second broken line gives the electron density at which the electrons begin to fill the second subband, or with $E_F = \min\{E_1(k_x)\}$.

4.2. Intersubband plasmons and FIR optical absorptions

The energies of the intersubband plasmons are determined by the solutions of the following equation:

$$\det\left|1 - \tilde{V}(q)\chi^{(0)}(q,\omega)\right| = 0. \tag{30}$$

Unlike the intrasubband plasmons, the energies of the intersubband plasmons do not approach zero as $q \to 0$ and are detectable by the FIR optical absorptions. The intersubband plasmons arise from the electron interactions between different subbands. This is seen from the definition of the matrix $\chi^{(0)}(q,\omega)$ in (17). When $q \to 0$ and $\hbar\omega \neq 0$, the factor $(N_{nk} - N_{n'k+q})/[E_n(k) - E_{n'}(k+q) + \hbar\omega + i0^+]$ in $\chi^{(0)}(q,\omega)$ is zero if $n = n'$.

To simplify the calculations, we will calculate the intersubband plasmons at $q = 0$ in the GaAs/AlAs PQWW with the interface structures given by (7) and the lowest subband occupied by the electrons. From the calculated subband structures (see figure 1), the following energy regions are defined:

$$\begin{aligned}
&0 < \Delta E^{(1)}_{\text{plasmon}} < \min\{E_1(k_x) - E_0(k_x)\} \\
&\min\{E_1(k_x) - E_0(k_x)\} < \Delta E^{(1)}_{\text{electron}} < \max\{E_1(k_x) - E_0(k_x)\} \\
&\max\{E_1(k_x) - E_0(k_x)\} < \Delta E^{(2)}_{\text{plasmon}} < \min\{E_2(k_x) - E_0(k_x)\} \\
&\min\{E_2(k_x) - E_0(k_x)\} < \Delta E^{(2)}_{\text{electron}} < \max\{E_2(k_x) - E_0(k_x)\}
\end{aligned} \tag{31}$$

and so on. The energy regions $\{\Delta E^{(n)}_{\text{electron}}\}$ are covered by the energies of the single-electron direct transitions from the lowest to high subbands, which will scatter the intersubband plasmons (with $q = 0$) and cause intersubband plasmon damping. Only in the energy regions $\{\Delta E^{(n)}_{\text{plasmon}}\}$, where single-electron direct transitions are forbidden, are the intersubband plasmons stable. In figure 7 we give the calculated results of the determinant $\text{Det}(\omega) = \det|1 - \tilde{V}(q)\chi^{(0)}(q,\omega)|_{q=0}$ as a function of $\hbar\omega$ for the PQWW with $L_z = 100\,\text{Å}$, $L_x = 400\,\text{Å}$, $\delta L_z = 30\,\text{Å}$ and $n_e = 3 \times 10^{11}\,\text{cm}^{-2}$. The energies at which $\text{Det}(\omega) = 0$ give the energies of the intersubband plasmons at $q = 0$. The shadowed regions in figure 7 are the regions of $\{\Delta E^{(n)}_{\text{electron}}\}$.

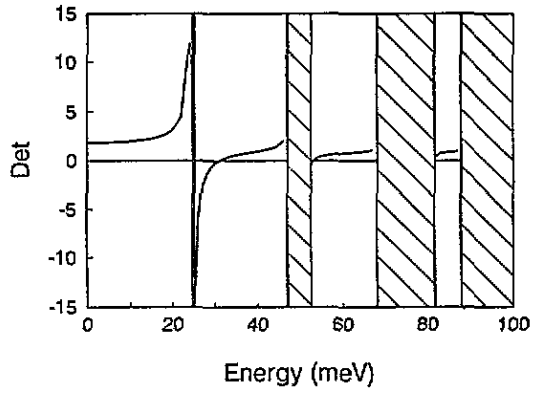

Figure 7. Numerical results of the determinant $\text{Det}(\omega) = \det|1 - \tilde{V}(q)\chi^{(0)}(q,\omega)|_{q=0}$ is given as a function of $\hbar\omega$ for the GaAs/AlAs PQWW with structural parameters $L_z = 100\,\text{Å}$, $L_x = 400\,\text{Å}$, $\delta L_z = 30\,\text{Å}$ and the electron density $n_e = 3 \times 10^{11}\,\text{cm}^{-2}$. The shaded regions are the regions where the intersubband plasmons at $q = 0$ will be scattered by single-electron direct transitions from the lowest to high electron conduction subbands.

No intersubband plasmons are found in the lowest region $\Delta E^{(1)}_{\text{plasmon}}$ and only one intersubband plasmon is found in each high region $\Delta E^{(n)}_{\text{plasmon}}$ $(n = 2, 3, \cdots)$. The energies of the intersubband plasmons become increasingly close to the transition energies of a single electron as the energies of intersubband plasmons increase. In what follows, we restrict our discussions to the lowest band of the intersubband plasmons in the region $\Delta E^{(2)}_{\text{plasmon}}$. In figure 8, we calculate the determinant $\text{Det}(\omega)$ as a function of $\hbar\omega$ for the PQWW with $L_z = 100\,\text{Å}$, $\delta L_z = 30\,\text{Å}$ and (*a*) $L_x = 400\,\text{Å}$, (*b*) $L_x = 300\,\text{Å}$ and (*c*) $L_x = 200\,\text{Å}$. The electron densities in the PQWW are $n_1 = 1 \times 10^{11}\,\text{cm}^{-2}$, $n_2 = 2 \times 10^{11}\,\text{cm}^{-2}$ and $n_3 = 3 \times 10^{11}\,\text{cm}^{-2}$. The energy region $\Delta E^{(2)}_{\text{plasmon}}$ is indicated in figure 8 by two broken lines. It is clear from figure 8 that the energies of the intersubband plasmons are well separated from the transition energies of the single electrons when the lateral period L_x of the PQWW increases ($L_x > 300\,\text{Å}$ for the PQWW we considered). By increasing the electron densities of the PQWW, we can increase the intersubband plasmon energies and shift them away from the energies of the single-electron direct transitions. This blue shift of the plasmon absorptions as the electron density increases has been observed in quantum wells and superlattices [37, 38].

It is interesting to know whether the FIR optical absorptions of the GaAs/AlAs PQWW are dominated by the intersubband plasmons or by single-electron direct transitions between different subbands. The FIR optical absorption coefficient $\alpha(\omega)$ of the PQWW is given by

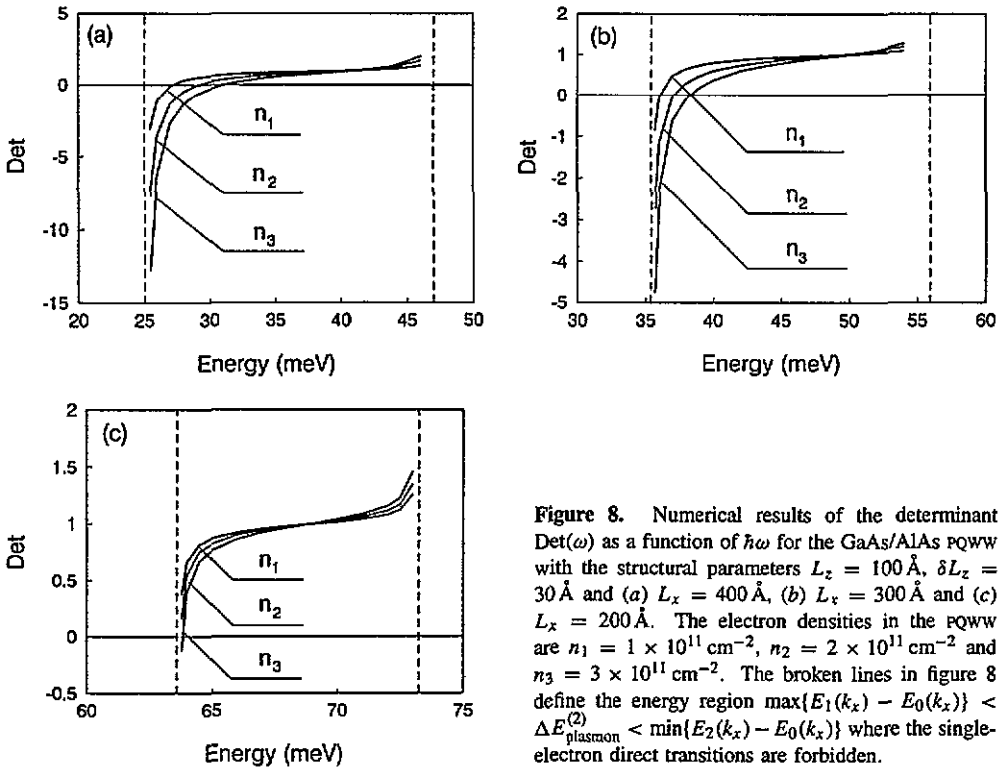

Figure 8. Numerical results of the determinant $\mathrm{Det}(\omega)$ as a function of $\hbar\omega$ for the GaAs/AlAs PQWW with the structural parameters $L_z = 100\,\text{Å}$, $\delta L_z = 30\,\text{Å}$ and (*a*) $L_x = 400\,\text{Å}$, (*b*) $L_x = 300\,\text{Å}$ and (*c*) $L_x = 200\,\text{Å}$. The electron densities in the PQWW are $n_1 = 1 \times 10^{11}\,\text{cm}^{-2}$, $n_2 = 2 \times 10^{11}\,\text{cm}^{-2}$ and $n_3 = 3 \times 10^{11}\,\text{cm}^{-2}$. The broken lines in figure 8 define the energy region $\max\{E_1(k_x) - E_0(k_x)\} < \Delta E^{(2)}_{\text{plasmon}} < \min\{E_2(k_x) - E_0(k_x)\}$ where the single-electron direct transitions are forbidden.

(12). But it is simpler to calculate the imaginary part of the complex dielectric function $\epsilon_2(\omega) = n(\omega)\alpha(\omega)c/\omega$, which is independent of the refractive index $n(\omega)$ of the PQWW. The incident light is assumed to propagate normally to the PQWW with the electric field polarized in the x direction. For electric fields polarized in the y direction, the FIR optical absorption is zero. In figure 9, we give the calculated $\epsilon_2(\omega)$ as a function of $\hbar\omega$ for the GaAs/AlAs PQWW with structural parameters (*a*) $L_z = 100\,\text{Å}$, $L_x = 200\,\text{Å}$, $\delta L_z = 30\,\text{Å}$, $n_e = 2 \times 10^{11}\,\text{cm}^{-2}$, (*b*) $L_z = 100\,\text{Å}$, $L_x = 300\,\text{Å}$, $\delta L_z = 30\,\text{Å}$, $n_e = 2 \times 10^{11}\,\text{cm}^{-2}$, and (*c*) $L_z = 70\,\text{Å}$, $L_x = 200\,\text{Å}$, $\delta L_z = 20\,\text{Å}$, $n_e = 3 \times 10^{11}\,\text{cm}^{-2}$. In figure 9 we also give the imaginary dielectric function $\epsilon_2^{(0)}(\omega)$ of the single electrons calculated by setting the electron interaction matrix $V(q) = 0$. In numerical calculations, we replace $\hbar\omega + \mathrm{i}0^+$ in (14)–(17) by $\hbar\omega + \mathrm{i}\eta$ with $\eta = 0.01\min\{E_1(k_x) - E_0(k_x)\}$. The parameter η accounts for the effect of the broadenings due to the disorder fluctuations of the PQWW structures, impurity scatterings, and so on. It also removes the irregular behaviour of $\chi^{(0)}(q)$ near the poles.

Two absorption peaks appear in $\epsilon_2^{(0)}(\omega)$, which correspond to single-electron transitions at the edge ($k_x/Q = 0.5$) and centre ($k_x/Q = 0$) of the FBZ with energies $\hbar\omega_1 = \min\{E_1(k_x) - E_0(k_x)\}$ and $\hbar\omega_2 = \max\{E_1(k_x) - E_0(k_x)\}$. The electron interactions cause redistributions of the absorption strengths. For the PQWW with a short lateral period ($L_x = 200\,\text{Å}$ in figure 9(*a*)), apart from a small redistribution of the absorption peaks, the effect of the intersubband plasmons is negligible. The FIR absorptions are dominated by single-electron direct transitions from subband $E_0(k)$ to $E_1(k)$. As the lateral period of the PQWW increases ($L_x = 300\,\text{Å}$ in figure 9(*b*)), the energies of the intersubband plasmons are well separated from those of the single-electron transitions. A strong intersubband plasmon absorption peak appears and becomes the dominant peak in the FIR optical absorption spectra

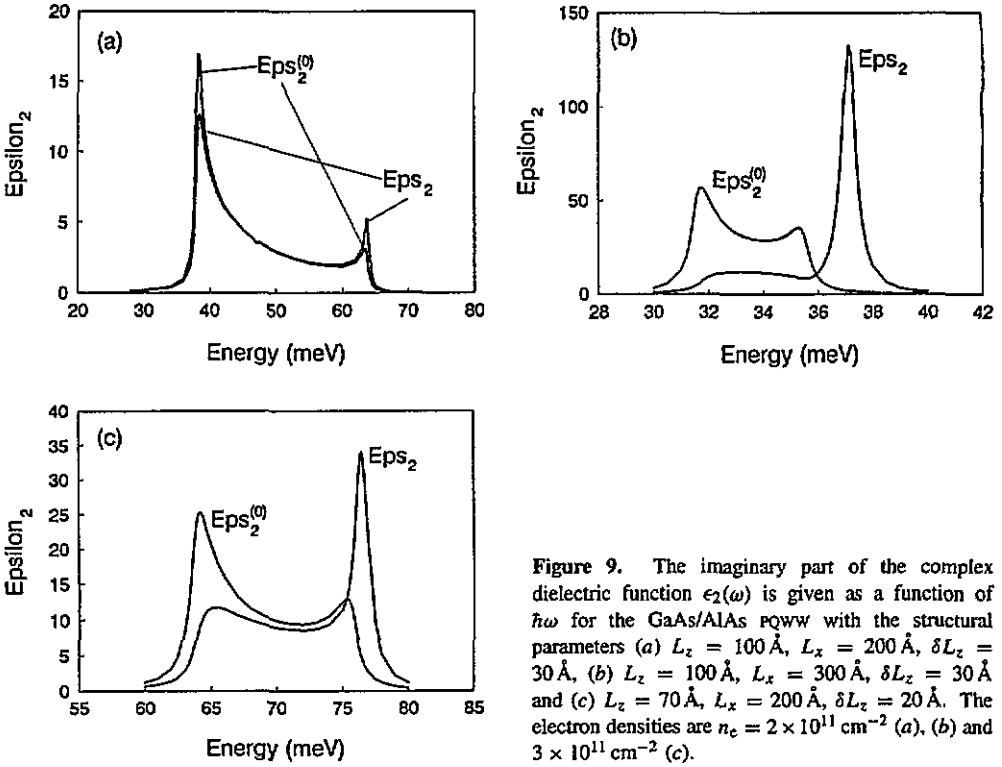

Figure 9. The imaginary part of the complex dielectric function $\epsilon_2(\omega)$ is given as a function of $\hbar\omega$ for the GaAs/AlAs PQWW with the structural parameters (*a*) $L_z = 100$ Å, $L_x = 200$ Å, $\delta L_z = 30$ Å, (*b*) $L_z = 100$ Å, $L_x = 300$ Å, $\delta L_z = 30$ Å and (*c*) $L_z = 70$ Å, $L_x = 200$ Å, $\delta L_z = 20$ Å. The electron densities are $n_e = 2 \times 10^{11}$ cm^{-2} (*a*), (*b*) and 3×10^{11} cm^{-2} (*c*).

of the PQWW. One should notice the different scales used in figure 9(*a*) and (*b*). The FIR absorptions in figure 9(*b*) have much stronger absorption peaks and much narrower widths than those in figure 9(*a*). The result in figure 9(*c*) shows that it is also possible that both single-electron transitions and intersubband plasmons contribute to the FIR optical absorptions of the PQWW. In our calculations we assumed, for simplicity, that the potential height between the well GaAs and barrier AlAs is infinite, which increases the strength of the lateral potential due to the periodically structured interfaces. We can reduce this increase in the strength of the lateral potential by assuming a smaller amplitude δL_z of the interface structures. Our calculations show that, except causing the peak positions to move to lower energies, the overall structures of $\epsilon_2(\omega)$ do not change when we reduce δL_z from 30 Å to 20 Å. In particular, the conditions under which the FIR absorptions are dominated by single-electron intersubband transitions and when by the intersubband plasmons are almost unchanged, and are determined mainly by the lateral period L_x of the PQWW.

5. Conclusions

The intrasubband and intersubband plasmons in the long-wavelength limit ($q \to 0$) were calculated numerically for the GaAs/AlAs PQWW produced by the deposition of GaAs and AlAs fractional layers on (001) vicinal GaAs substrates. One intrasubband plasmon mode was found, the energy of which approaches zero as the in-plane wave vector $q \to 0$. The dispersion relations of the intrasubband plasmons are anisotropic with $\hbar\omega_p = [(\alpha^2 q_x^2 + \alpha_0^2 q_y^2)/q]^{1/2}$. The constant α_0 increases monotonically with the electron

density n_e of the PQWW, while α increases with n_e when the Fermi energy E_F lies within the subbands and decreases with n_e when E_F is in the gaps of the subbands. The intersubband plasmons were found to be multi-branch structured with non-zero energies as $q \to 0$. The calculations show that for the GaAs/AlAs PQWW we considered where the lateral periods L_x of the PQWW are much less than 200 Å, the FIR optical absorptions are dominated by single-electron direct transitions between different subbands. For PQWW with L_x larger than 300 Å, the absorptions are due to intersubband plasmon absorptions. In between these two regions, both single-electron direct transitions and intersubband plasmon absorptions can make important contributions to the absorptions, depending on the structures of the PQWW.

Acknowledgments

H Sun acknowledges support by the National Natural Science Foundation of China under Grant No. 19274035 and the Science and Technology Foundation of High Education of China. K W Yu acknowledges support from the University and Polytechnic Grant of Hong Kong under project 221-300-150.

Appendix A

If we define the matrix $D(q,\omega) = V(q)\chi^{(0)}(q,\omega) = \{D_{l_1l_2,l_1'l_2'}(q+Q_m, q+Q_m', \omega)\}$, the elements of the determinant $\det|1 - V(q)\chi^{(0)}(q,\omega)| = \det|1 - D(q,\omega)|$ are given, using the definition of $V(q)$ in (22), by

$$\delta_{l_1,l_1'}\delta_{l_2,l_2'}\delta_{m,m'} - D_{l_1l_2,l_1'l_2'}(q+Q_m, q+Q_m', \omega) = \delta_{l_1,l_1'}\delta_{l_2,l_2'}\delta_{m,m'} - \delta_{l_1,l_2}\delta_{m,0}\frac{2\pi e^2}{\epsilon S_0 q}\sum_{l}\chi^{(0)}_{ll,l_1'l_2'}(q, q+Q_m', \omega) - \tilde{D}_{l_1l_2,l_1'l_2'}(q+Q_m, q+Q_m', \omega) \tag{A1}$$

where $\tilde{D}(q,\omega) = \tilde{V}(q)\chi^{(0)}(q,\omega) = \{\tilde{D}_{l_1l_2,l_1'l_2'}(q+Q_m, q+Q_m', \omega)\}$. The value of $\det|1 - D(q,\omega)|$ is not changed if we add the column (l_1', l_1', Q_0) to column $(1, 1, Q_0)$ of the determinant. Thus the elements in the column $(1, 1, Q_0)$ become

$$\sum_{l_1'}\{\delta_{l_1,l_1'}\delta_{l_2,l_1'}\delta_{m,0} - D_{l_1l_2,l_1'l_1'}(q+Q_m, q+Q_0, \omega)\} = \delta_{l_1,l_2}\delta_{m,0} \times\left(1 - \frac{2\pi e^2}{\epsilon S_0 q}\sum_{ll'}\chi^{(0)}_{ll,l'l'}(q, q, \omega)\right) - \sum_{ll'Q}\tilde{V}_{l_1l_2,ll'}(q+Q_m, q+Q)\sum_{l_1'}\chi^{(0)}_{ll',l_1'l_1'}(q+Q, q, \omega). \tag{A2}$$

From (25) we find that, in the long-wavelength limit ($q \to 0$), the second term on the right-hand side of (A2) contributes to the energy of the plasmons with an order of magnitude of q and can be neglected. We also notice that the second term on the right-hand side of (A1) and the first term on the right-hand side of (A2) are either zero or independent of the row index $(l_1l_2Q_m)$. Mapping the row and column indexes $(l_1l_2Q_m, l_1'l_2'Q_m')$ of the determinant

elements in (A1) and (A2) one-to-one to positive integers (i, j), we obtain the following equations for $\det|1 - D(q, \omega)|$:

$$\det|1 - D(q,\omega)| = d_1 \begin{vmatrix} 1 & d_2 + d_{1,2} & d_3 + d_{1,3} & \cdots & d_j + d_{1,j} & \cdots \\ 1 & d_2 + d_{2,2} & d_3 + d_{2,3} & \cdots & d_j + d_{2,j} & \cdots \\ \vdots & \vdots & \vdots & \cdots & \vdots & \vdots \\ 1 & d_2 + d_{k,2} & d_3 + d_{k,3} & \cdots & d_j + d_{k,j} & \cdots \\ 0 & d_{k+1,2} & d_{k+1,3} & \cdots & d_{k+1,j} & \cdots \\ \vdots & \vdots & \vdots & \cdots & \vdots & \vdots \\ 0 & d_{i,2} & d_{i,3} & \cdots & d_{i,j} & \cdots \\ \vdots & \vdots & \vdots & \cdots & \vdots & \vdots \end{vmatrix} \tag{A3}$$

$$= d_1 \begin{vmatrix} 1 & d_{1,2} & d_{1,3} & \cdots & d_{1,j} & \cdots \\ 1 & d_{2,2} & d_{2,3} & \cdots & d_{2,j} & \cdots \\ \vdots & \vdots & \vdots & \cdots & \vdots & \vdots \\ 1 & d_{k,2} & d_{k,3} & \cdots & d_{k,j} & \cdots \\ 0 & d_{k+1,2} & d_{k+1,3} & \cdots & d_{k+1,j} & \cdots \\ \vdots & \vdots & \vdots & \cdots & \vdots & \vdots \\ 0 & d_{i,2} & d_{i,3} & \cdots & d_{i,j} & \cdots \\ \vdots & \vdots & \vdots & \cdots & \vdots & \vdots \end{vmatrix}$$

$$= \left(1 - \frac{2\pi e^2}{\epsilon S_0 q} \sum_{ll'} \chi^{(0)}_{ll,l'l'}(q, q, \omega)\right) \det|1 - \tilde{V}(q)\, \chi^{(0)}(q, \omega)|$$

where

$$d_1 = \left(1 - (2\pi e^2/\epsilon S_0 q) \sum_{ll'} \chi^{(0)}_{ll,l'l'}(q, q, \omega)\right)$$

is the non-zero element on the right-hand side of (A2) which is mapped to the first column in (A3), d_j $(j = 2, 3, \cdots)$ represent the non-zero elements of the second term on the right-hand side of (A1), which is independent of the row index $(l_1 l_2 Q_m)$, and $d_{i,j}$ represent the first and third terms on the right-hand side of (A1). The second equality in (A3) is obtained by multiplying the first column with $-b_j$ $(j = 2, 3, \cdots)$ and adding it to the jth column. By definition, the determinant behind the second equality of (A3) can be obtained from $\det|1 - V(q)\, \chi^{(0)}(q, \omega)|$ by replacing the matrix $V(q)$ with $\tilde{V}(q)$, then adding all the columns $(l'_1 l'_1 Q_0)$ to column $(11Q_0)$ and following the discussions after (A2). The last manipulation does not change the value of $\det|1 - \tilde{V}(q)\chi^{(0)}(q, \omega)|$ and we arrive at the final equality in (A3).

References

[1] Petroff P M, Gossard A G and Wiegmann W 1984 *Appl. Phys. Lett.* **45** 620
[2] Warren A C, Antoniadis D A, Smith H I and Melngailis J 1985 *IEEE Electron. Device Lett.* **6** 294
[3] Fukui T and Saito H 1987 *Appl. Phys. Lett.* **50** 824
[4] Tanaka M and Sakaki H 1988 *Japan. J. Appl. Phys.* **27** L2025

[5] Fukui T and Saito H 1988 *J. Vac. Sci. Technol.* B **6** 1373
[6] Gaines J M, Petroff P M, Kroemer H, Simes R J, Geels R S and English J H 1988 *J. Vac. Sci. Technol.* B **6** 1478
[7] Motohisa J, Tanaka M and Sakaki H 1989 *Appl. Phys. Lett.* **55** 1214
[8] Weiss D, Klitzing K V, Ploog K and Weimann G 1989 *Europhys. Lett.* **8** 117
[9] Gerhardts R R, Weiss D and Klitzing K V 1989 *Phys. Rev. Lett.* **62** 1173
[10] Winkler R W and Kotthaus J P 1989 *Phys. Rev. Lett.* **62** 1177
[11] Tsuchiya M, Gaines J M, Yan R H, Simes R J, Holtz P O, Coldren L A and Petroff P M 1989 *Phys. Rev. Lett.* **62** 466
[12] Ismail K, Chu W, Yen A, Antoniadis D A and Smith H I 1989 *Appl. Phys. Lett.* **54** 460
[13] Tanaka M and Sakaki H 1989 *Appl. Phys. Lett.* **54** 1326
[14] Kohl M, Heitmann D, Grambow P and Ploog K 1990 *Phys. Rev.* B **42** 2941
[15] Sugawara H, Schulman J H and Sakaki H 1991 *J. Appl. Phys.* **69** 2722
[16] Stormer H J, Pfeiffer L N, Baldwin K W, West K W and Spector J 1991 *Appl. Phys. Lett.* **58** 726
[17] Kern K, Demel T, Heitmann D, Grambow P, Zhang Y H and Ploog K 1991 *Superlatt. Microstruct.* **9** 11
[18] Smoliner J, Rosskopf V, Berthold G, Gornik E, Böhm G and Weimann G 1992 *Phys. Rev.* B **45** 1915
[19] Fukui T, Tsubaki K, Saito H, Kasu M and Honda T 1992 *Surf. Sci.* **267** 588
[20] Nötzel R, Ledentsov N N and Ploog K 1992 *Phys. Rev.* B **45** 3507
[21] Mackens U, Heitmann D, Prager L, Kotthaus J P and Beinvogl W 1984 *Phys. Rev. Lett.* **53** 1485
[22] Demel T, Heitmann D, Grambow P and Ploog K 1988 *Phys. Rev.* B **38** 12732
[23] Demel T, Heitmann D, Grambow P and Ploog K 1990 *Phys. Rev. Lett.* **64** 788
[24] Kern K, Heitmann D, Grambow P, Zhang Y H and Ploog K 1991 *Phys. Rev. Lett.* **66** 1618
[25] Lorke A, Jejina I and Kotthaus J P 1992 *Phys. Rev.* B **46** 12845
[26] Cataudella V 1988 *Phys. Rev.* B **38** 7828
[27] Li Q and Sarma S D 1990 *Phys. Rev.* B **41** 10268
[28] Que W 1991 *Phys. Rev.* B **43** 7127
[29] Park P W, MacDonald A H and Schaich W L 1992 *Phys. Rev.* B **46** 12635
[30] Latgé A and Castro J A 1993 *Phys. Rev.* B **47** 4798
[31] Kim N and Uloa S E 1993 *Phys. Rev.* B **48** 11987
[32] Levine B F, Choi K K, Bethea C G, Walker J and Malik R J 1988 *Appl. Phys. Lett.* **50** 1092
[33] Johnson N F, Ehrenreich H and Jones R V 1988 *Appl. Phys. Lett.* **53** 180
[34] Sun H 1992 *Phys. Rev.* B **46** 12371
[35] Madelung O 1978 *Introduction to Solid-State Physics* (Berlin: Springer) p 266
[36] Que W 1993 *Phys. Rev.* B **47** 1636
[37] Pinczuk A, Schmitt-Rink S, Danan G, Valladares J P, Pfeiffer L N and West K W 1989 *Phys. Rev. Lett.* **63** 1633
[38] Manasreh M O, Szmulowicz F, Vaughan T, Evans K R, Stutz C E and Fischer D W 1991 *Phys. Rev.* B **43** 9996